Protein Engineering of Xylose (Glucose) Isomerase from *Actinoplanes missouriensis*. 1. Crystallography and Site-Directed Mutagenesis of Metal Binding Sites[†,‡]

John Jenkins,[§,∥] Joël Janin,[§] Felix Rey,[§] Mohammed Chiadmi,[§] Herman van Tilbeurgh,[⊥,#] Ignace Lasters,[○,△] Marc De Maeyer,[○,△] Daniel Van Belle,[○] Shoshana J. Wodak,[×] Marc Lauwereys,[⊥,△] Patrick Stanssens,[⊥,△] Nadir T. Mrabet,[⊥,▽] Johan Snauwaert,[⊥,+] Gaston Matthyssens,[⊥,△] and Anne-Marie Lambeir*[,⊥,△]

Laboratoire de Biologie Physicochimique, CNRS UA1131, Bâtiment 433, Université Paris-Sud, F-91405 Orsay, France, Plant Genetic Systems N.V., Jozef Plateaustraat 22, B-9000 Gent, Belgium, and PGS/UCMB and UCMB, Université Libre de Bruxelles, Avenue Paul Hêger P2, B-1050 Brussels, Belgium

Received October 17, 1991; Revised Manuscript Received February 26, 1992

ABSTRACT: The structure and function of the xylose (glucose) isomerase from *Actinoplanes missouriensis* have been analyzed by X-ray crystallography and site-directed mutagenesis after cloning and overexpression in *Escherichia coli*. The crystal structure of wild-type enzyme has been refined to an *R* factor of 15.2% against diffraction data to 2.2-Å resolution. The structures of a number of binary and ternary complexes involving wild-type and mutant enzymes, the divalent cations Mg^{2+}, Co^{2+}, or Mn^{2+}, and either the substrate xylose or substrate analogs have also been determined and refined to comparable *R* factors. Two metal sites are identified. Metal site 1 is four-coordinated and tetrahedral in the absence of substrate and is six-coordinated and octahedral in its presence; the O2 and O4 atoms of linear inhibitors and substrate bind to metal 1. Metal site 2 is octahedral in all cases; its position changes by 0.7 Å when it binds O1 of the substrate and by more than 1 Å when it also binds O2; these bonds replace bonds to carboxylate ligands from the protein. Side chains involved in metal binding have been substituted by site-directed mutagenesis. The biochemical properties of the mutant enzymes are presented. Together with structural data, they demonstrate that the two metal ions play an essential part in binding substrates, in stabilizing their open form, and in catalyzing hydride transfer between the C1 and C2 positions.

D-Xylose isomerase (EC 5.3.1.5) catalyzes the isomerization of the five-carbon aldose D-xylose to the ketose D-xylulose. It also converts D-glucose, a six-carbon analog of D-xylose, to D-fructose in a reaction that is industrially applied to the production of high-fructose corn syrup. For this reason, D-xylose isomerase is widely known as glucose isomerase, even though the kinetic parameters are less favorable for the six-carbon than for the five-carbon substrate. Aldose–ketose isomerization requires divalent metal cations such as Mg^{2+}, Co^{2+}, or Mn^{2+}. Bacterial xylose isomerases have four identical subunits with molecular weights near 43 000. X-ray studies of the enzymes from several *Streptomyces* species have shown that they have very similar three-dimensional structures (Carrell et al., 1984, 1989; Henrick et al., 1987, 1989; Farber et al., 1987; Rey et al., 1988; Dauter et al., 1989; Whitlow et al., 1991), consistent with a high degree of sequence homology. Each subunit folds into a main domain which has a typical "triose-phosphate isomerase barrel" motif with an eight-stranded parallel β-sheet surrounded by eight α-helices and a C-terminal helical domain which forms a large loop embracing a neighboring subunit. The active site is located near the center of the barrel, as it is in triose-phosphate isomerase and in other enzymes that contain a parallel β-barrel.

The reactions catalyzed by xylose isomerase and triose-phosphate isomerase are similar, and they have the same stereochemistry (Rose, 1981). Yet, their mechanism is different. Triose-phosphate isomerase, which does not require metal cations, uses base catalysis to shuttle a proton between the C1 and C2 positions of the substrate (Alber et al., 1981). As the active site of xylose isomerase contains no properly positioned base to do so, an alternative mechanism based on a 1,2-hydride shift has been proposed by Farber et al. (1989). It has received strong support from a series of X-ray structures of *Arthrobacter* (Collyer et al., 1990) and of *Streptomyces rubiginosus* (Whitlow et al., 1991) xylose isomerases.

We have carried out an analysis of the enzyme from *Actinoplanes missouriensis*, by protein engineering techniques combining molecular genetics and biochemical and structural studies of the wild-type enzyme cloned and expressed in *Escherichia coli*, and of a number of mutant enzymes obtained by site-directed mutagenesis. Protein engineering of *A. missouriensis* xylose isomerase has led to the production of enzymes with enhanced heat stability (Mrabet et al., 1992). We present here structural and biochemical data which provide further information on the catalytic mechanism and the role of metal ions. The data include the X-ray structure of wild-

[†] This work is part of the Protein Engineering Project between Plant Genetic Systems N.V., Gist-Brocades N.V. (Delft, Holland), and Amylum N.V. (Aalst, Belgium) supported by GIMV (Gewestelijke Investeringsmaatschappij Vlaanderen).

[‡] The coordinates of the structures have been deposited in the Brookhaven Protein Data Bank under the file names 1XIM, 2XIM, 3XIM, 4XIM, 5XIM, 6XIM, and 7XIM.

* Author to whom correspondence should be addressed.

[§] CNRS UA1131.

[∥] Present address: AFRC Institute of Food Research, Shinfield, Reading RG2 9AT, England.

[⊥] Plant Genetic Systems N.V.

[#] Present address: LCCMB, Faculté de Médecine Nord, Boulevard Pierre Dramard, F-13326 Marseille 15, France.

[○] PGS/UCMB, Université Libre de Bruxelles.

[△] Present address: Corvas International, N.V., J. Plateaustraat 22, D-9000 Gent, Belgium.

[×] UCMB, Université Libre de Bruxelles.

[▽] Present address: LEGG/URA–CNRS 457, Université de Nancy I, Nancy, France.

[+] Present address: LCBD, KU Leuven, Celestijnenlaan 200D, B-3001 Heverlee, Belgium.

0006-2960/92/0431-5449$03.00/0

type and mutant enzymes alone or in the presence of Mg^{2+} or Co^{2+} ions, of the substrate xylose, of the linear substrate analogs xylitol and sorbitol, and of several cyclic inhibitors. The inhibitors, and the substrate which is bound in the open conformation, are closely associated with the metal ions. We discuss functional and structural properties of mutant enzymes in which some of the metal ligands are substituted. Accompanying papers describe other mutant xylose isomerases and details of the catalytic mechanism.

Materials and Methods

Protein Sample Preparation and Enzymatic Assay. Isolation, cloning, and expression in *E. coli* of the *A. missouriensis* (DSM 43046) xylose isomerase gene will be described elsewhere (P. Stanssens and M. Lauwereys, personal communication). The gene carried by pMac vectors was used for oligonucleotide-directed mutagenesis by the gapped duplex method; wild-type and mutant enzymes were produced in soluble form in *E. coli* strain K527 harboring the pMa5-I plasmid (Stanssens et al., 1989). Enzyme purification will be described in detail elsewhere (M. Lauwereys, personal communication). Briefly, it involves heating the bacterial lysate for 30 min at 70 °C, centrifugation and ammonium sulfate fractionation of the supernatant, Phenyl-Superose chromatography with a reverse ammonium sulfate gradient, gel permeation on Sephacryl S 200 HR, and Mono-Q anion-exchange chromatography with a NaCl gradient from 0 to 0.6 M.

Enzymic activity was determined using sorbitol dehydrogenase as an auxiliary enzyme (Kersters-Hilderson et al., 1987) in 50 mM triethanolamine (TEA) buffer, pH 7.5. Enzymic activity could not be determined in mutant enzymes having less than 0.5% wild-type activity. Steady-state parameters were measured at 35 °C for xylose and at 60 °C for glucose, in the presence of either 10 mM Mg^{2+}, 1 mM Co^{2+}, or 1 mM Mn^{2+}. D-Xylose concentration was varied between 1 and 100 mM for K_M and k_{cat} determination and glucose concentration between 10 mM and 1 M.

Crystallization and Ligand Soaks. Recombinant wild-type and mutant xylose isomerases expressed in *E. coli* crystallized under conditions similar to those described by Rey et al. (1988) for the wild-type enzyme isolated from *A. missouriensis*. Purified protein (25 mg/mL) in 1 M ammonium sulfate and 0.1 M sodium phosphate buffer, pH 6.9–7.1, was placed in hanging drops over pits containing 1.2 M ammonium sulfate. The final pH was about 6.8. Crystals grew to large sizes (up to 1 mm^3) in a period of weeks at 18 °C.

Metal ions and ligands were added by soaking crystals in solutions containing 0.1 M MOPS buffer, pH 6.9, 1.7 M ammonium sulfate, metal salt, and ligands for a few hours before mounting in glass capillaries for diffraction data collection. Mineral salts, substrates D-glucose and D-xylose, and open-chain inhibitors xylitol and sorbitol were from Merck. Cyclic inhibitor 1,5-anhydroxylitol was prepared according to Saman et al. (1972) and β-D-pseudoglucose [5-(hydroxymethyl)-1,2,3,4-cyclohexanetetrol], according to Ogawa et al. (1985); α-D-pseudoxylose, also called (1*S*)-dihydroconduritol F, was synthesized by reduction of pyrogallol (L. Dumortier, personal communication; see also Dumortier et al. (1989) for part of the synthetic route).

Diffraction Data Collection. All crystals tested so far were isomorphous and had cell parameters very close to those described by Rey et al. (1988) for the wild-type enzyme extracted from *A. missouriensis*, except for mutant H290N, which gave crystals with a slightly longer *c* axis. The crystals belong to trigonal space group $P3_221$ and have a tetramer (MW 144 000) in the asymmetric unit. The cell parameters are $a = b = 143.45$ Å, $c = 231.50$ Å, $\alpha = \beta = 90°$, and $\gamma = 120°$.

Diffraction data were collected with synchrotron radiation at LURE-DCI (Orsay, France), using monochromatic radiation near 1.4-Å wavelength and an Arndt-Wonacott rotation camera from ENRAF-Nonius. Crystals were cooled to 4 °C during collection in order to improve stability in the beam. A typical data set included 50 packs of three Kodak DE5 films, each pack representing a 0.8° oscillation about the *c* axis. As the minimum rotation range is 30° in this space group, the data sets were sufficiently redundant. Because of the long *c* axis, a crystal-to-film distance of 80 mm was used, effectively limiting the resolution to 2.2 Å. Limited exposure time and crystal decay further restricted the useful resolution of some of the data sets.

Films were digitized on an Optronics film scanner and processed with the program DENZO (Otwinowski, Yale University, New Haven, CT). Further data reduction used the CCP4 package (CCP4, Daresbury, England). An empirical absorption correction (Stuart & Walker, 1979) was applied using calculated structure factors as reference. Statistics on data sets discussed below are given in Table I.

Crystallographic Refinement. All crystallographic refinement was carried out with the FFT version of the PROLSQ restrained least-squares refinement program (Hendrickson & Konnert, 1980; Hendrickson, 1985), running on DEC VAX computers. Model building used the FRODO program of Jones (1985) installed on a PS300 graphic system from Evans & Sutherland. Structural parameters for open-chain ligands were derived from the crystal structure of xylitol (Kim & Jeffrey, 1969).

The initial model of xylose isomerase described by Rey et al. (1988) was built from a 2.8-Å electron density map phased with single isomorphous replacement and noncrystallographic symmetry. This model was refined against data set 1 collected in the presence of xylitol. Refinement brought the *R* factor down to 26% at 2.2-Å resolution with no manual intervention. At this stage, the model was examined in detail, part of it was rebuilt, solvent molecules were progressively added, and refinement was pursued. Noncrystallographic symmetry restraints (Leslie, 1987), which had been applied during early steps of refinement, were removed after the *R* factor dropped below 20%. The total number of refinement cycles was over 250.

The final model derived from data Set 1 has an *R* factor of 15.2% at 2.2-Å resolution and excellent geometry (Table I). It contains 12 212 protein atoms from residues 3–394, 40 ligand atoms, and 8 metal ions located at the four active sites, plus 881 water molecules. Residues 1 and 2 could not be located in the electron density map and were not built. All other models were obtained by PROLSQ refinement starting from this model and with the same geometric restraints. Refinement was straightforward in most cases, the only manual intervention required being the substitution of mutated side chains and the addition or removal of ligand and solvent molecules. Refinement statistics are all very similar. The *R* factor dropped from initial values of 20–25% to near 15% in about 20 cycles. As the average atomic displacement is of the order of 0.2 Å, all refined structures are essentially identical except at specific locations.

Atomic occupancy was not refined. Full occupancy was assumed throughout refinement for all atoms including solvent, with a few exceptions. During refinement of model 1, the low electron density and high *B* factor of metal 2 suggested incomplete saturation. Additional cycles were carried out with

Table I: Diffraction Data and Crystallographic Refinement

data set	1	2	3	4	5	6	7	8	9	10
crystals										
protein[a]	WT	WT	WT	WT	WT	WT	WT	WT	triple KR	K253R
ligand[b]	xylitol	sorbitol			xylose	pseudoxylose	pseudoglucose	anhydroxylitol	sorbitol	xylose
metal[c]	(Co)	Mg	Co	EDTA, pH 5	Mg	Co	Mg	Mg	Co	Mg
data collection										
resolution (Å)	2.2	2.6	2.3	2.4	2.5	2.3	2.2	2.3	2.3	2.3
no. of crystals	6	6	4	7	6	5	7	6	5	5
film packs	52	51	48	43	56	52	57	62	44	54
reflections: total	255 106	151 955	225 965	191 464	180 487	231 740	257 142	299 414	254 909	240 939
reflections: independent	122 049	73 491	108 255	102 663	85 490	107 630	118 923	116 119	95 937	108 522
R merge (%)[b]	6.0	6.6	6.2	8.1	5.9	5.4	6.2	8.8	5.9	7.3
refinement										
R factor (%)[e]	15.2	14.4	15.2	15.8	15.1	14.7	15.8	15.6	14.9	14.9
reflections	113 145	71 972	107 023	92 378	84 028	98 870	114 547	114 268	95 937	108 519
protein atoms	12 260	12 264	12 158	12 172	12 260	12 246	12 220	12 229	12 276	12 268
solvent	881	868	837	895	881	853	904	877	871	919
distances (Å)[f]										
bonds lengths (1–2) [0.02]	0.011	0.013	0.011	0.013	0.011	0.012	0.011	0.011	0.011	0.011
bond angles (1–3) [0.04]	0.038	0.042	0.039	0.042	0.0389	0.041	0.038	0.039	0.039	0.038
planar groups (1–4) [0.04]	0.037	0.040	0.039	0.040	0.035	0.039	0.036	0.037	0.037	0.037
nonbonded [0.50]	0.266	0.266	0.267	0.268	0.267	0.268	0.264	0.268	0.267	0.267
planarity (Å) [0.01]	0.010	0.010	0.010	0.010	0.009	0.010	0.010	0.010	0.010	0.009
chiral vol (Å^3) [0.15]	0.127	0.135	0.130	0.135	0.127	0.131	0.126	0.125	0.128	0.128
av *B* (Å^2)	21.1	19.6	20.6	21.2	19.8	19.0	18.7	18.2	18.8	18.2

data set	11	12	13	14	15	16	17	18	19	20
crystals										
protein[a]	E181Q	D255A	H220N	H290N	D257K	E186Q	E186Q	A25K	M88S/H243N	F61K
ligand[b]	xylose	xylose	xylose	sorbitol	xylose	xylose	xylose	xylitol	xylitol	glucose
metal[c]	Mg	Mg	Mg	Co	Co	Mg	Mn	Mg	Co	Mg
data collection										
resolution (Å)	2.3	2.3	2.4	2.3	2.3	2.4	2.4	2.3	2.5	2.5
no. of crystals	7	5	6	4	5	7	3	4	3	4
film packs	62	54	71	40	55	42	30	48	32	31
reflections: total	272 287	220 605	286 552	239 000	247 346	244 294	183 803	263 454	182 284	142 841
reflections: independent	108 856	99 074	103 387	98 930	107 888	97 974	93 032	94 632	79 999	59 916
R merge (%)[d]	6.7	5.2	5.7	5.8	6.3	6.3		8.0	6.1	9.2
refinement										
R factor (%)[e]	15.3	15.2	15.5	15.4	15.3	14.6	14.4	15.7	15.1	15.5
reflections	107 427	97 681	101 894	97 899	106 487	97 974	85 586	93 283	78 919	58 821
protein atoms	12 212	12 244	12 248	12 260	12 260	12 232	12 235	12 262	12 242	12 220
solvent	904	881	889	900	882	981	978	869	898	865
distances (Å)[f]										
bonds lengths (1–2) [0.02]	0.011	0.011	0.012	0.011	0.012	0.010	0.011	0.012	0.011	0.011
bond angles (1–3) [0.04]	0.038	0.039	0.041	0.039	0.040	0.036	0.039	0.040	0.038	0.039
planar groups (1–4) [0.04]	0.036	0.036	0.038	0.036	0.039	0.035	0.038	0.038	0.034	0.035
nonbonded [0.50]	0.267	0.264	0.265	0.271	0.266	0.265	0.266	0.267	0.269	0.276
planarity (Å) [0.01]	0.010	0.010	0.010	0.009	0.010	0.009	0.010	0.010	0.009	0.009
chiral vol (Å^3) [0.15]	0.127	0.127	0.132	0.128	0.132	0.126	0.130	0.131	0.129	0.133
av *B* (Å^2)	19.9	17.5	17.5	21.2	17.4	16.8	18.1	20.4	16.5	19.0

[a] Xylose isomerase in data set 1 was isolated from *A. missouriensis*; all other data sets used protein expressed in *E. coli*. [b] Ligands were soaked at the following concentrations: xylitol, 0.2 M; sorbitol, 0.5 M; D-xylose, 0.5 M; α-D-pseudoxylose, 1.9 M; β-D-pseudoglucose, 0.5 M; 1,5-anhydroxylitol, 1.25 M. Buffer was 0.1 M MOPS, pH 7.0, except in data sets 1 and 4, where phosphate buffer was used. [c] Metal salts were soaked at the following concentrations: $MgSO_4$, 25 mM except 100 mM in data sets 12 and 13; $CoCl_2$, 10 mM; $MnCl_2$, 10 mM. No metal was added to the protein used for data set 1. High density at both metal sites indicated the presence of a metal ion, presumably Co^{2+} carried over from the *A. missouriensis* extract. Data set 4 was collected in the presence of 25 mM EDTA on protein extensively dialyzed against EDTA. [d] Merging *R* factor: $R_{merge} = \sum_i\sum_j|I_{ij} - I_i|/\sum_i\sum_j I_{ij}$. [e] *R* factor as given by PROLSQ including all independent reflections to the quoted resolution limit. [f] Input standard deviations in brackets and rms deviations from input parameters. Distances between second neighbors (1–3 distances) restrain bond angles; distances between second neighbors (1–4 distances) restrain planar groups. Nonbonded distances refer to multiple-torsion contacts. Restraints were also applied to other contacts, to torsion angles, and to *B* factors.

occupancy factors of 0.5 and 0.75; the first value led to reasonable *B* factors and was kept. The same procedure was applied to ligand atoms when needed. For these atoms, occupancy and *B* factors are highly correlated, and neither is a reliable quantity.

Accuracy of X-ray Structures. The accuracy of the atomic positions in refined model 1 is estimated to be about 0.15 Å on average, on the basis of the dependence of *R* on resolution (Luzzati, 1952). The rms amplitude of atomic vibrations calculated from average *B* factors near 20 Å^2 (Table I) is about 0.5 Å. *B* factors are significantly larger at the N-terminus up to residue 9 and for residues 278–284. An independent estimate of accuracy makes use of the noncrystallographic 222 symmetry of the tetramer. It is obtained by comparing positions of equivalent atoms in the four subunits and measuring distances from their average position. Departure from 222 symmetry was negligible (0.05 Å rms) during steps of refinement where noncrystallographic symmetry restraints were applied. It remained low after these restraints were removed. The rms distance from 222 averaged positions in refined model

FIGURE 1: Metal sites of xylose isomerase. View of the Cα chain trace of a xylose isomerase subunit. The active site is in the TIM barrel, which opens toward the center of the tetramer in front. Metal site 2 (dark sphere) is above site 1 (light sphere).

1 is only 0.17 Å for all protein atoms. This is comparable to the error estimate based on the *R* factor, implying that the four subunits are essentially identical. Discrepancies larger than 1 Å affect a few surface side chains and many solvent molecules. The four active sites strictly obey local symmetry: equivalent metal positions in all four subunits superimpose to within 0.1 Å rms. Moreover, *B* factors are lower than average in these parts of the crystal structure, for which the 0.15-Å estimated accuracy is probably realistic. Atomic positions and distances quoted below are given as an average with a standard deviation calculated over four independent values.

We compared our model of *A. missouriensis* xylose isomerase to that of the *Arthrobacter* enzyme studied at 2.3-Å resolution by Henrick et al. (1989) and deposited at the Brookhaven Protein Data Bank (file 4XIA; Bernstein et al., 1977). The two proteins share 67% sequence identity, with a single residue insertion near position 280 in the *Arthrobacter* sequence relative to *A. missouriensis*. Omitting residues 278–284, Cα atoms in subunits of the two proteins superimpose to within 0.60 Å rms. An rms discrepancy of 0.75 Å is expected for two well-refined protein models with 67% sequence identity (Chothia & Lesk, 1986). We can thus conclude that both xylose isomerase models are of high quality and that the two molecules are closely similar, except for residues 278–284, which form a loop with different conformations in the two structures and are poorly ordered in ours.

Results

Metals and Substrate Binding Sites. Figure 1 is an overview of the xylose isomerase subunit, showing the TIM barrel and the large C-terminal loop that constitute each subunit. The active site, located deep in the middle of the barrel, opens toward the front. It includes two metal binding sites and a closely associated substrate binding site. The metal binding sites are labeled sites 1 and 2 following Carrell et al. (1989) and Collyer et al. (1990). Site 1 is the "structural" site of Whitlow et al. (1991); site 2, their "catalytic" site.

The metal sites are empty in the wild-type enzyme structure that we determined in the presence of EDTA (model 4). In other structures reported here, they are occupied by Co^{2+} or Mg^{2+}. A mutant structure with Mn^{2+} is described in the accompanying paper by van Tilbeurgh et al. (1992). As can be seen in Figure 2, Co^{2+} occupies both sites with remarkably little change in the protein. Mg^{2+} does the same. However, Mg^{2+}, which has only 10 electrons, can be confused with solvent unlike Co^{2+}, which is easily identified in electron density maps. Replacement of Mg^{2+} with a water molecule or NH_4^+, which is present at 3.4 M concentration in the

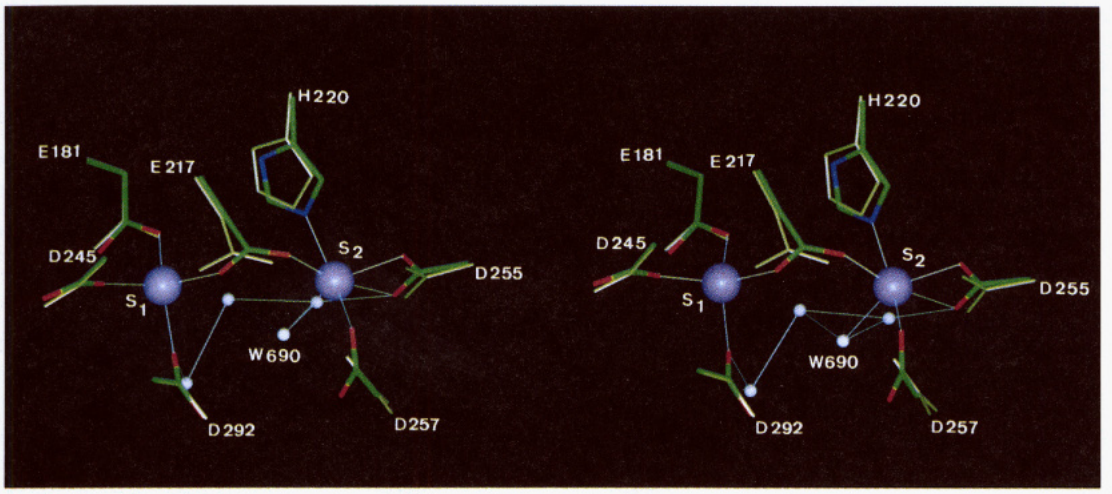

FIGURE 2: Metal sites with and without bound metal. Stereo diagram showing the superposition of the active site in the presence of Co^{2+} [model 3, where relevant side chains are shown with their bonds colored according to atomic types: oxygens (red), nitrogens (blue), and carbons (green); Co^{2+} ions are shown as purple spheres and the water molecules as small white spheres; bonds made by the metals and H-bonds among and to displayed water molecules are shown as thin white lines] and in the absence of metal (model 4, relevant side chains are displayed in light green). The water molecules are from the Co^{2+} structure. Metal sites 1 and 2 are labeled S_1 and S_2, respectively.

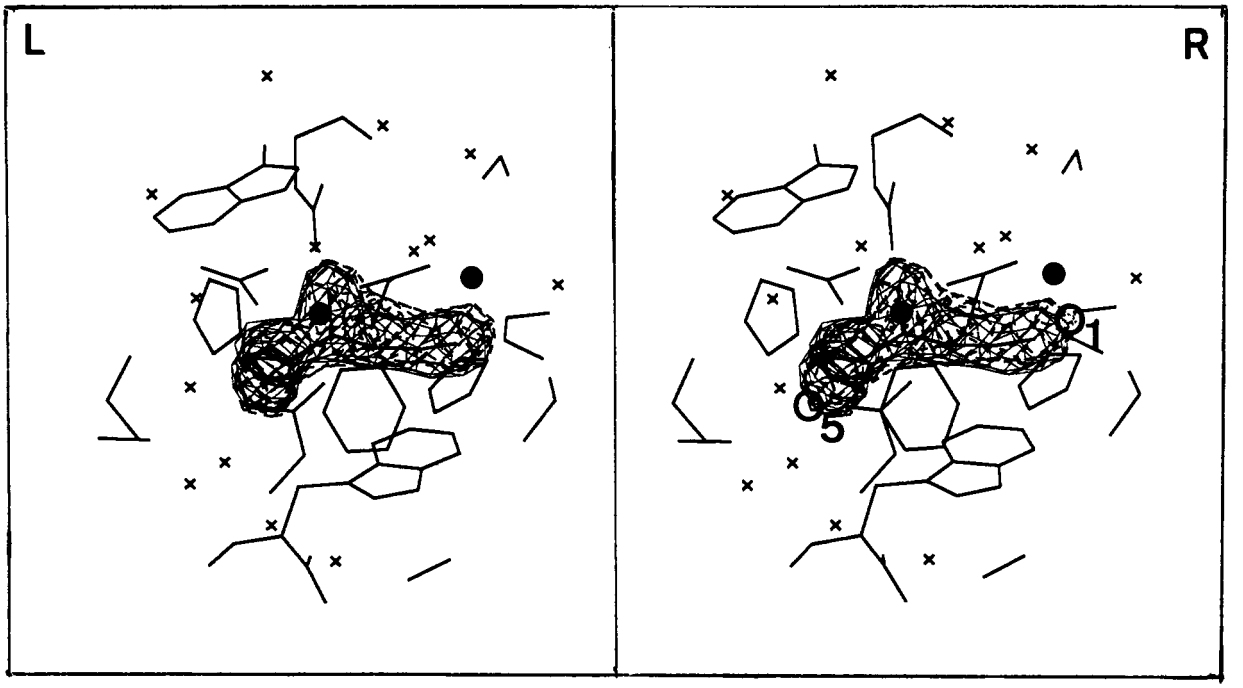

FIGURE 3: Xylitol and xylose at the active site. $F_o - F_c$ electron densities are calculated for xylitol in model 2 (dashes) and xylose in model 10 (full lines) omitting the ligand from F_c; the density is contoured at 6σ. Heavy dots are metal positions; crosses, water molecules. The xylose density is slightly flatter at C2, which suggests that xylose is in equilibrium with xylulose.

mother liquor, should increase the distance to oxygen ligands from about 2.1 Å to standard H-bond lengths of 2.6–3 Å. On this basis, site 1 appears to be fully occupied by Mg^{2+} but not site 2, as will be discussed below.

Substrate and inhibitor binding is detailed in the accompanying paper by Lambeir et al. (1992). We find that the electron density for bound xylose is consistently similar to that of the linear inhibitor xylitol (Figure 3). We see no evidence of the cyclic pyranose form of the sugar. On the other hand, some D-xylulose product of the enzymic conversion of added xylose may be present at the active site. The equilibrium favors xylose in solution, but Whitlow et al. (1991) see xylulose as the majority species at the active site of the *S. rubiginosus* enzyme. Since the chemical nature of the sugar cannot be decided upon the sole basis of 2.2–2.4-Å electron density maps, it was built as xylitol. Cycles of PROLSQ refinement were performed with no chirality restraint on the C2 atom in model 10. The chiral volume was refined to 50 ± 30% of the value expected for a tetrahedral carbon, which may indicate that both xylose and xylulose are present at the active site. However, a distortion of the planar C_2 geometry of xylulose or the tetrahedral geometry of xylose induced by binding to the metal would also explain these findings.

Inhibitors 1,5-anhydroxylitol, α-D-pseudoxylose, and β-D-pseudoglucose were chosen as models of cyclic substrates; 1,5-anhydroxylitol has no hydroxyl in position 2; in the other two compounds, the ring oxygen is replaced with a methylene group. Pseudoxylose binding was observed in model 6, but no density for β-pseudoglucose was found in the map of model 7, probably because the enzyme is specific for α-anomers. In model 8, 1,5-anhydroxylitol had poor electron density due to low occupancy and could be built confidently only in one of the four subunits.

Metal Site 1. Metal site 1 is formed by the four carboxylates of Glu 181, Glu 217, Asp 245, and Asp 292. These residues are located on β-strands 5, 7, and 8 of the TIM barrel, well inside the barrel. Each carboxylate donates an oxygen atom to the metal. Average metal–oxygen bond lengths are listed in Table II with standard deviations calculated over the four subunits. They are near 2.0 Å, implying direct coordination. In model 7, slightly longer bonds may indicate incomplete occupancy of the metal site by Mg^{2+} when the substrate site is empty. Otherwise, bond lengths fit well with small molecule crystal structures reviewed by Carrell et al. (1988). Average metal–carboxylate bond lengths in these structures are 2.04 Å for Mg^{2+}, 2.06 Å for Co^{2+}, and 2.16 Å for Mn^{2+}. In xylose isomerase, we observe 2.09 ± 0.06 Å (average and standard deviation of all bonds to metal 1), with no significant difference between Mg^{2+}, Co^{2+}, and Mn^{2+}. The bond to Glu 181 is slightly longer (2.18 Å) than the other three, which average 2.07 Å.

When the substrate site is empty, we find metal 1 to be four-coordinated. This is illustrated for Co^{2+} in model 3 and for Mg^{2+} in model 7. The coordination geometry of Co^{2+} in model 3 is clearly tetrahedral, the metal being 0.5 Å out of the plane defined by oxygens of Glu 181, Asp 245, and Asp 292 (Figure 4). No water molecule is closer than 3.2 Å. In complexes with open-chain ligands, additional bonds are made and the metal is six-coordinated. Xylitol, sorbitol, and xylose/xylulose interact with the metal through O2 and O4. The metal–oxygen bond length is 2.3 ± 0.1 Å, larger than with the carboxylates. The geometry is octahedral; the metal ion is in a plane containing O2, O4, and the oxygens of Glu 217 and Asp 245. It has moved by 0.4 Å relative to its previous position, toward the substrate and away from Glu 217. The movement is significant, as the rms dispersion of metal 1 positions in xylitol or xylose complexes is only 0.08 Å.

Cyclic inhibitors α-pseudoxylose and 1,5-anhydroxylitol bind next to metal 1. Their O3 and O4 hydroxyl oxygens are less than 3 Å from the metal, in a plane that also contains oxygens of Glu 217 and Asp 245. Though this would fit into an octahedral geometry, the oxygens of Glu 181 and Asp 292 are not aligned on the metal as they are in complexes with open-chain ligands, and the four carboxylate ligands are still tetrahedrally arranged around the metal.

Metal Site 2. Metal site 2 is located less than 5 Å from site 1, nearer the surface of the TIM barrel. Residues involved in this site belong to β-strands 6 and 7 and to the loops con-

Table II: Metal Ligand Geometry, Site 1[a]

data set	3	1	6	9	19	14	15	17
metal–ligand	Co	Co–xylitol	Co–PSX	Co–sorbitol	Co–xylitol	Co–sorbitol	Co–xylose	Mn–xylose
protein	WT	WT	WT	triple	M88S/H243N	H290N	D257K	E186Q
geometry	tetrahedral	octahedral	tetrahedral	octahedral	octahedral	octahedral	octahedral	octahedral
distance (Å) to atom								
Glu 181 OE2	2.20 (0.05)	2.26 (0.05)	2.22 (0.08)	2.18 (0.08)	2.17 (0.09)	2.16 (0.06)	2.17 (0.09)	2.17 (0.04)
Glu 217 OE2	1.95 (0.08)	2.20 (0.06)	2.05 (0.06)	2.08 (0.07)	2.07 (0.07)	2.06 (0.06)	2.10 (0.06)	1.99 (0.04)
Asp 245 OD2	1.94 (0.02)	2.24 (0.02)	2.11 (0.05)	2.10 (0.03)	2.13 (0.10)	2.12 (0.10)	2.08 (0.04)	2.09 (0.03)
Asp 292 OD1	2.06 (0.08)	2.20 (0.08)	2.00 (0.10)	2.04 (0.06)	2.15 (0.02)	2.07 (0.04)	2.07 (0.01)	2.07 (0.10)
sugar O2		2.28 (0.06)		2.40 (0.12)	2.16 (0.10)	2.28 (0.07)	2.31 (0.04)	2.25 (0.09)
sugar O4		2.46 (0.04)	2.98 (0.07)	2.38 (0.05)	2.27 (0.03)	2.18 (0.04)	2.32 (0.07)	2.35 (0.04)
sugar O3			2.56 (0.28)					

data set	7	2	5	10	18	12	13	8	16
metal–ligand	Mg	Mg–sorbitol	Mg–xylose	Mg–xylose	Mg–xylitol	Mg–xylose	Mg–xylose	Mg–AHX	Mg–xylose
protein	WT–PSG	WT	WT	K253R	A25K	D255A	H220N	WT	E186Q
geometry	tetrahedral	octahedral	octahedral	octahedral	octahedral	octahedral	octahedral	tetrahedral	octahedral
distance (Å) to atom									
Glu 181 OE2	2.36 (0.13)	2.18 (0.08)	2.18 (0.08)	2.08 (0.03)	2.15 (0.08)	2.17 (0.03)	2.16 (0.06)	2.26 (0.04)	2.15 (0.06)
Glu 217 OE2	2.20 (0.05)	2.07 (0.06)	2.09 (0.05)	2.05 (0.04)	2.10 (0.04)	2.05 (0.05)	2.03 (0.03)	1.94 (0.08)	2.04 (0.03)
Asp 245 OD2	2.25 (0.03)	2.10 (0.01)	2.11 (0.03)	2.08 (0.07)	2.11 (0.02)	2.07 (0.02)	1.98 (0.03)	2.20 (0.09)	2.02 (0.05)
Asp 292 OD1	2.19 (0.1)	2.17 (0.04)	2.09 (0.05)	2.09 (0.10)	2.06 (0.05)	2.03 (0.06)	1.99 (0.07)	2.06 (0.10)	2.02 (0.07)
sugar O2		2.26 (0.06)	2.35 (0.11)	2.30 (0.03)	2.21 (0.11)	2.33 (0.07)	2.35 (0.07)		2.24 (0.07)
sugar O4		2.15 (0.05)	2.30 (0.06)	2.41 (0.08)	2.30 (0.05)	2.39 (0.07)	2.42 (0.07)	2.7[b]	2.21 (0.02)
sugar O3								3.1	

[a] Distances less than 3.4 Å from the metal ion to ligand atoms. Values quoted are the average and standard deviation (in parentheses) of the values observed at the four active sites of the tetramer, which are crystallographically independent. [b] Due to low occupancy, 1,5-anhydroxylitol was built only at one of four active sites.

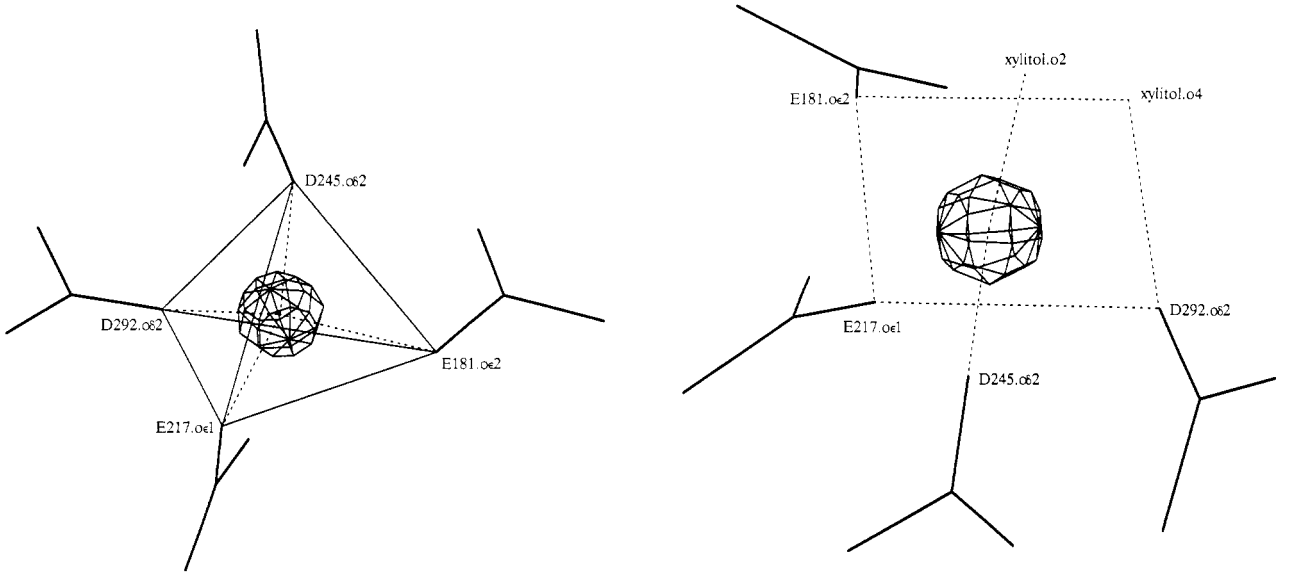

FIGURE 4: Coordination geometry of metal site 1. In the absence of substrate and inhibitor (model 4, left), Co^{2+} is four-coordinated and tetrahedral. In the presence of substrate or of a linear inhibitor (xylitol in model 1, right), it is six-coordinated and octahedral.

necting these β-strands to the next α-helices in the barrel. The carboxylates of Glu 217, Asp 255, and Asp 257, the imidazole group of His 220, and a well-defined water molecule (water 690) constitute this site. The site is destroyed by the mutation in the D257K, D255A, and H220N proteins. In all other structures, metal 2 is at least six-coordinated and its geometry is octahedral, although we shall see that some of the ligands do exchange. Table III lists bond lengths. They are generally longer and more disperse than for site 1, probably because site 2 is incompletely occupied in several data sets. Carboxylate–Mg^{2+} bonds range from 2 to 3 Å. The larger value suggests that the metal is replaced with solvent in models 2 (wild-type–sorbitol complex) and 18 (A25K mutant–xylose complex). In contrast, Co^{2+} and Mn^{2+} fully occupy site 2 except in model 1. The coordination geometry is more regular than with Mg^{2+}, and the bonds are shorter. The metal–nitrogen bond to His 220 is 2.3 Å long; metal–oxygen distances are 2.07 Å to Glu 217 and 2.20 Å to water 690.

When the substrate binding site is empty (models 3 and 7) or occupied by cyclic inhibitors (models 6 and 8), the bond to Asp 257 is short (2.10 Å) and that to Asp 255 is bidentate. The bidentate bond may be somewhat longer (2.23 Å) than the others. Cyclic inhibitors do not bind to the metal at site 2, and they do not affect it. Open-chain substrates and inhibitors do so through their O1 atom. The distance from O1 to the metal is 2.65 ± 0.2 Å. In models 9, 19, 14, and 16, O2 is also within 3 Å of metal 2 and can also be considered as a ligand. Thus, the substrate gives either one or two bonds to metal 2.

When the substrate binds, metal 2 moves and some of its bonds to the protein are lost. The movement is toward the substrate, away from Asp 257 and orthogonal to the bond to Glu 217. The bonds to Asp 255 and Asp 257 break; those to Glu 217, His 220, and water 690 are maintained as the metal carries with it the solvent molecule and the side chain of His 220. These movements are illustrated on Figures 5 and 6. We

Table III: Metal Ligand Geometry, Site 2[a]

data set	3	1	6	9	19	14	15	17
metal–ligand	Co	Co–xylitol	Co–PSX	Co–sorbitol	Co–xylitol	Co–sorbitol	Co–xylose	Mn–xylose
protein	WT	WT	WT	triple	M88S/H243N	H290N	D257K	E186Q
position	2_0	2_1[b]	2_0	2_2	2_2	2_2	*c*	2_0
distance (Å) to atom								
Glu 217 OE1	2.02 (0.08)	2.29 (0.06)	2.04 (0.04)	2.11 (0.07)	2.09 (0.17)	2.11 (0.11)		2.06 (0.04)
His 220 NE2	2.39 (0.08)	2.75 (0.03)	2.39 (0.07)	2.30 (0.06)	2.25 (0.08)	2.23 (0.04)		2.70 (0.05)
Asp 255 OD1	2.20 (0.07)	2.38 (0.10)	2.23 (0.07)	2.47 (0.12)				2.02 (0.20)
Asp 255 OD2	2.21 (0.07)	2.53 (0.06)	2.22 (0.04)					2.77 (0.23)
Asp 257 OD1	2.11 (0.06)	2.82 (0.11)	2.27 (0.06)	3.17 (0.12)				2.45 (0.08)
water 690	2.10 (0.04)	2.28 (0.04)	2.10 (0.07)	2.28 (0.03)	2.31 (0.10)	2.25 (0.07)		
sugar O1		2.80 (0.09)		2.67 (0.14)	2.31 (0.10)	2.28 (0.07)		
sugar O2				2.54 (0.16)	2.20 (0.08)	2.05 (0.09)		
water 694					2.30 (0.12)	2.24 (0.05)		

data set	7	2	5	10	18	12	13	8	16
metal–ligand	Mg	Mg–sorbitol	Mg–xylose	Mg–xylose	Mg–xylose	Mg–xylose	Mg–xylose	Mg–AHX	Mg–xylose
protein	WT–PSG	WT	WT	K253R	A25K	D255A	H220N	WT	E186Q
position	2_0	*c*	2_1	2_1	*c*	*c*	*c*	2_0	2_1[c]
distance (Å) to atom									
Glu 217 OE1	2.03 (0.10)		2.14 (0.08)	2.46 (0.08)	3.10 (0.15)			2.27 (0.10)	2.27 (0.10)
His 220 NE2	2.64 (0.07)		2.50 (0.04)	2.83 (0.10)	3.25 (0.11)			2.74 (0.06)	2.48 (0.11)
Asp 255 OD1	2.23 (0.11)		2.72 (0.10)	2.52 (0.13)	2.94 (0.03)			2.26 (0.10)	
Asp 255 OD2	2.07 (0.04)		2.73 (0.06)	2.86 (0.05)	2.70 (0.13)			2.39 (0.08)	
Asp 257 OD1	2.54 (0.09)		3.00 (0.08)	2.92 (0.11)	2.93 (0.30)			2.51 (0.10)	3.35 (0.12)
water 690	2.14 (0.04)		2.09 (0.11)	2.10 (0.10)	3.00 (0.09)			2.24 (0.16)	2.28 (0.06)
sugar O1			2.56 (0.09)	2.73 (0.18)	2.97 (0.14)				2.40 (0.08)
sugar O2			3.20 (0.28)						2.40 (0.08)
water 694									2.96 (0.22)

[a] Distances less than 3.4 Å from the metal ion to ligand atoms. Values quoted are the average and standard deviation (in parentheses) of the values observed at the four active sites of the tetramer, which are crystallographically independent. The last line is the distance to metal 1. [b] Occupancy was adjusted to 0.5. [c] Metal was absent or low occupancy. Distances quoted for model 18 refer to a solvent molecule replacing the metal.

Table IV: Catalytic Parameters of Xylose Isomerase Mutants Directed to Metal Binding Sites

	xylose[a]		glucose[b]		cation activation[c]				
					K_{act}			relative activity	
	k_{cat} (s^{-1})	K_M (mM)	k_{cat} (s^{-1})	K_M (M)	Mg (mM)	Co (μM)	Mn (μM)	Co/Mg	Mn/Mg
WT	17.3	4.8	24.9	0.29	0.08	8.4	4.8	0.46	0.40
E181A	no activity								
E181S	no activity								
E181D	1.5	73	9.3	2.4	7.3	85	4	0.51	0.20
E181Q	0.1	50			5.1	770	270	1.0	2.5
E217D	no activity								
E217Q	no activity								
E217S	0.08							8.3	60
D245A	no expression								
D245L	no expression								
D245N	no activity								
D292A	no activity								
D292E	no activity								
D292N	no activity								
D255A	no activity								
D255E	no expression								
D255N	0.5	66			3.4	<50	23	0.16	1.9
D257A	no expression								
D257K	no activity								
D257S	no activity								
D257E	3.4	48	17.7	5.8	0.9	8	4	0.35	0.12
D257N	0.9	49	5.0	0.3	3.4				
H220N	0.05		0.2	0.5					
H220Q	0.6	16	0.7	0.4	0.3				

[a] Kinetic parameters with substrate xylose are determined at 35 °C in the presence of 10 mM $MgSO_4$ (20 mM for D255N and 100 mM for E181Q). No expression: no overexpression of the mutant in *E. coli*. No activity: less than 0.5% of wild-type activity. [b] Kinetic parameters with glucose are determined at 60 °C in the presence of 10 mM $MgSO_4$. [c] K_{act} is the metal ion concentration that yields 50% of maximum activity with 0.2 M xylose at 35 °C; the relative activity is the ratio of the maximum activity achieved with Co^{2+} or Mn^{2+} compared to Mg^{2+}.

shall name site 2_0 the position observed in the ligand-free protein and in complexes with cyclic inhibitors; the subscript indicates that no bond is made to the substrate. Site 2_0 is the same to within 0.11 Å rms in five structures containing Co^{2+} (models 3 and 6), Mg^{2+} (models 7 and 8), or Mn^{2+} (model 17). In structures where the metal interacts with O1 (models 1, 5, and 10), a second position is observed, which we call site 2_1. It is the same to within 0.18 Å rms in all three models, and it is located 0.7 Å from site 2_0 (Figure 5). When it is at site 2_1, the metal makes four short bonds to protein ligands and water 690 and longer bonds to Asp 255 and Asp 257. Last, there are three structures where Co^{2+} binds to both O1

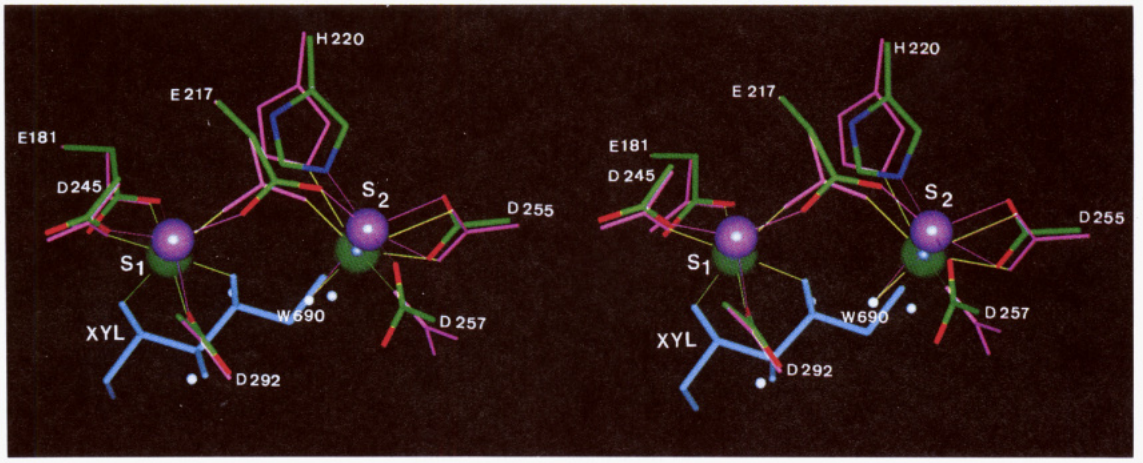

FIGURE 5: Metal movement upon substrate binding. Stereo diagram displaying the superposition of the active site of the wild-type enzyme in the presence of Co^{2+} [model 3, where relevant side chains are shown with their bonds colored according to atomic types: oxygens (red), nitrogens (blue), and carbons (green); Co^{2+} ions are shown as purple spheres and the water molecules as small white spheres; bonds made by the metals are displayed as thin purple lines] and of the K253R thermostable mutant with xylose and Mg^{2+} (model 10, where relevant side chains are displayed in magenta; Mg^{2+} ions are shown as green spheres and water molecules as small white spheres, and xylitol is displayed in light blue; bonds made by Mg^{2+} ions are in light yellow). Metal 1 (S_1) on the left moves toward the substrate and binds to O2 and O4. Metal 2 (S_2) moves from site 2_0 to site 2_1 and binds to O1. The substrate displaces the water molecules from the Co^{2+} structure.

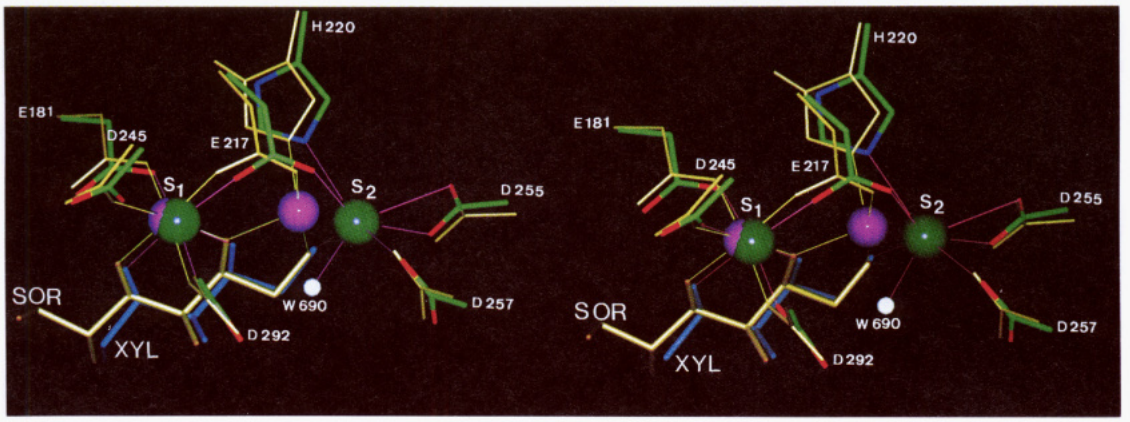

FIGURE 6: Metal movement from site 2_1 to site 2_2. Stereo diagram showing the superposition of the active site of the K253R–xylose–Mg^{2+} [model 10, where relevant side chains are displayed with their bonds colored according to atom types: oxygens (red), nitrogens (blue), and carbons (green); Mg^{2+} ions are displayed as green spheres and water molecules as small white spheres; bonds made by the metal are shown in magenta; the bound xylitol is shown in light blue] and of the H290N–sorbitol–Co^{2+} complexes (model 14, relevant side chains and the bound sorbitol are displayed in gold; the Co^{2+} ions are shown as magenta spheres, and the bonds made to them are in gold). Sorbitol binds to metal 1 (S_1) in the same way as a hexose in open form; compared to xylose, it has an additional CH_2OH group apparent on the left. Both its O1 and O2 coordinate with metal 2 (S_2), which is now at site 2_2 and no longer binds to Asp 255 and Asp 257.

and O2 (models 9, 19, and 14). They define site 2_2, located 1.2 Å away from site 2_0 and 0.6 Å from site 2_1 (Figure 6). When the metal ion is bound at site 2_2, the bonds with Asp 255 and Asp 257 are broken.

Mutations Directed toward Metal Site 1. We substituted by site-directed mutagenesis each of the residues involved in metal binding. Table IV describes the effects of these substitutions on the enzymic activity toward xylose and glucose, on the apparent affinity of the enzyme for Mg^{2+}, Co^{2+}, and Mn^{2+}, and on the relative efficiency of the three cations as activators. Catalytic parameters quoted for mutant enzymes can be compared to those of the wild-type enzyme measured under the same conditions.

Removing any of the four carboxylates that bind metal 1 has a dramatic effect on activity. None of the Asp 245 and Asp 292 mutant enzymes are active. Two mutants of Glu 217 and Glu 181 retain residual activity near the 0.5% limit of detection: E217S and E181Q. Enzyme E217S has very low activity in the presence of Mg^{2+}, but it is more active in the presence of Co^{2+} and Mn^{2+}. When Glu 181 is replaced with an aspartate (E181D), the protein retains about 10% activity on xylose and 40% on glucose, but with a high K_M and a low apparent affinity for Mg^{2+}. Thus, the negative charge is essential at position 181, but it can move slightly, while it cannot do so at position 217.

In enzyme E181Q, the negative charge of the carboxylate is lost, yet the Gln side chain, which is sterically equivalent to Glu, can conceivably bind the metal through the amide oxygen. The residual activity is low, but the change in K_M excludes the possibility that it is due to deamidation of the glutamine. We determined the X-ray structure of this enzyme in the presence of xylose and Mg^{2+} (model 11). Significant differences from the wild-type enzyme were observed only in the vicinity of the active site. The side-chain amide of Gln 181 was found in position to interact with the carboxylate of Asp 245. No density attributable to metal was observed at either cation site, and no substrate was bound, which is consistent with the observed 100-fold reduction in affinity for Mg^{2+} and the 10-fold increase in K_M for xylose.

Mutations Directed toward Metal Site 2. Mutations affecting metal site 2 are less crippling. Asp 257 is replaced with a glutamate in the D257E enzyme which has 20% activity on

xylose and 70% on glucose, again with high K_M and low apparent affinity for Mg^{2+}. Replacing the negative charge of either Asp 255 or Asp 257 with an amide that can still ligate the metal ion yields enzymes D255N and D257N, which have significant activity (3–5%) on xylose with low apparent affinities for substrate and Mg^{2+}. Other substitutions abolish expression or activity. The X-ray structure of the D257K enzyme, which is inactive and where a positive charge from the engineered lysine replaces metal 2, will be described elsewhere (Jenkins et al., personal communication).

Removing the side chain of His 220 by substituting an alanine yields the inactive H220A enzyme. The more conservative substitution with Asn or Gln leaves detectable activity. The H220Q enzyme has about 3% activity on both xylose and glucose; its K_M and apparent affinity for Mg^{2+} are less perturbed than for any other mutant quoted in Table IV. The X-ray structures of the D255A and H220N enzymes were determined in the presence of xylose and Mg^{2+} (models 12 and 13). In both, site 1 was occupied by Mg^{2+} and the substrate was bound in open form in the usual way, but site 2 appeared to contain only solvent. Apart from the obvious absence of the Asp 255 side chain, only minor changes were observed in the D255A enzyme structure. Water molecules replace the missing carboxylate. Lys 183 hydrogen bonds to one of them instead of the carboxylate. In the H220N enzyme, the asparagine side chain was found to replace the imidazole with minimal perturbations.

Discussion

After we identified two adjacent metal ion sites in *A. missouriensis* xylose isomerase in a heavy atom derivative with the trivalent ion Eu^{3+} (Rey et al., 1988), inhibitor and substrate binding studies confirmed that the metals are intimately involved in substrate binding and catalysis. The X-ray analysis of other xylose isomerases led to the same conclusion. Mg^{2+} binding to the *Arthrobacter* enzyme was described by Henrick et al. (1989); other divalent and trivalent metal ions were described by Collyer et al. (1990). The metal sites of *S. rubiginosus* xylose isomerase have been described by Carrell et al. (1989) and Whitlow et al. (1991). We now compare these structures with ours.

In the presence of open-chain ligands, metal site 1 is apparently identical in *A. missouriensis*, *Arthrobacter*, and *S. rubiginosus*: octahedral coordination to four carboxylate oxygens of equivalent residues and to O2 and O4 of the ligand. Bond lengths given here in Table II are essentially the same as those determined at 1.6-Å resolution on the *S. rubiginosus* enzyme by Whitlow et al. (1991). Binding of the cyclic inhibitor 5-thioglucose is described by Collyer et al. (1990); the inhibitor interacts with the metal through O3 and O4. We observe pseudoxylose and 1,5-anhydroxylitol in the same position. We diverge, however, on the metal geometry in the absence of substrate or inhibitor. Collyer et al. (1990) assume that site 1 remains octahedral as solvent molecules replace hydroxyls. Water molecules bound to metal 1 of *S. rubiginosus* xylose isomerase are mentioned by Carrell et al. (1989) and by Whitlow et al. (1991). Yet, we find no water molecule within 3 Å of metal 1 under similar circumstances, and its geometry is tetrahedral.

In *Arthrobacter* and *S. rubiginosus* xylose isomerases, different positions of site 2 have been described. In the *Arthrobacter* enzyme, Collyer et al. (1990) see the metal in positions 2 and 2′. In position 2, it binds to residues equivalent to Glu 217, His 220, and Asp 257 and to a water molecule, and it makes a bidentate bond to Asp 255. This corresponds exactly to our metal site 2_0. Position 2′ is about 1 Å away from position 2. It is taken by Mg^{2+} in a complex where site 1 is occupied by Al^{3+}. Mg^{2+} binds O1 and O2; bonds to Asp 257 and Asp 255 are broken. These features are those of metal site 2_2, about 1.2 Å away from site 2_0. In the crystal structure of the *S. rubiginosus* enzyme in complex with Mn^{2+} and xylose, Mn^{2+} has two alternative positions 1.76 Å apart; only the one with lower occupancy binds to the substrate (Whitlow et al., 1991).

We observe Co^{2+} at site 2_2 with linear inhibitors bound to three mutant enzymes (models 9, 14, and 19). In other X-ray data sets collected under similar circumstances, the metal is at site 2_1 halfway from site 2_0, and it binds only to O1. The mutation sites are remote from metal 2, and the active sites of the mutant enzymes are essentially like those of the wild type. The mutant enzyme used in model 9, which has three surface lysine residues changed to arginine, differs from the wild type only in being more stable at high temperature (Mrabet et al., 1992). The lysine–arginine substitutions are not expected to influence metal binding. We conclude that the position of metal 2 and its coordination are extremely sensitive to the environment. The only permanent bonds are to Glu 217, His 220, and water 690. Metal 2 can move 1–1.5 Å while making these bonds and maintaining an octahedral geometry. The movement is in a direction that does not affect the bond to Glu 217. That to His 220 is maintained through a simple rotation of the side chain, and the water molecule follows the metal.

Visible light spectroscopy studies of Co^{2+} binding to xylose isomerases of *Streptomyces violaceoruber* (Callens et al., 1988) and *S. rubiginosus* (Sudfelt et al., 1990) detect the presence of a high-affinity site with octahedral geometry and a low-affinity site with tetrahedral or pentacoordinated geometry. Magnetic circular dichroism also indicates that the two sites have different geometries in the absence of substrate or inhibitors and that they become octahedral in their presence (Sudfelt et al., 1990). This is consistent with our description of metal site 1. Carrell et al. (1989) and Whitlow et al. (1991) describe both metal sites of the *S. rubiginosus* enzyme as octahedral and six-coordinated even without substrate. The metal is Mn^{2+} in this case. The discrepancy may result from a difference between Co^{2+} and Mn^{2+}, between enzymes, or between experimental conditions, pH in particular.

Metal ion binding at both sites is required for enzymic activity. All available structural data on all xylose isomerases show that metal 1 binds to the substrate in cyclic form through O3 and O4 and in open form through O2 and O4. Shorter metal–oxygen bonds and a more favorable octahedral geometry in the second case may be the driving force for ring opening. It should nevertheless be mentioned that Whitlow et al. (1991) have evidence for substrate binding in the absence of metal, largely as the cyclic species. We can confirm that metal 2 is not required for substrate binding and ring opening, as we see xylose bound in open form to two mutant enzymes where site 2 is destroyed: D255A and D257K. The unusual flexibility of this site may be required for the metal to remain bound to O1 while the geometry of the C1 atom changes from trigonal in xylose or glucose to tetrahedral in xylulose and fructose. Moreover, metal 2 is essential for isomerization. This involves a hydride transfer between C2 and C1 and a proton transfer between O2 and O1. The strong electric field from both cations should contribute significantly to lower the energy barrier for the hydride transfer. As for the proton transfer, a likely mechanism involves the water molecule that is tightly bound to metal 2 (Whitlow et al., 1991; van Tilbeurgh et al., 1992).

Our biochemical data on mutants where either site is modified provide further information on cation binding. In those which retain activity, the apparent affinity for the cations decreases by 2 orders of magnitude, as in E181Q, D255N, or D257N. The apparent affinity for the substrate, judged from K_M values, decreases by 1 order of magnitude. These substitutions have qualitatively similar effects on Mg^{2+}, Co^{2+}, and Mn^{2+} despite the much higher affinity of the enzyme for the last two metals. Quantitative differences between cations are nevertheless apparent when the Co/Mg activity ratio is compared, which can be higher (E181Q) or lower (D255N) than in the wild type. Asp/Glu substitutions in E181D and D257E affect the apparent affinity for Co^{2+} and Mn^{2+} much less than they do for Mg^{2+} and for the substrates (Table IV). The reason for such differential effects between cations is clear for the E186Q mutant enzyme: its X-ray structure shows a perturbed geometry of the metal binding site in the presence of Mg^{2+}, which returns essentially back to the wild-type structure in the presence of Mn^{2+}, presumably due to its high affinity for the site (van Tilbeurgh et al., 1992). This interpretation can be extended to other mutant enzymes which are poorly activated by Mg^{2+}.

ACKNOWLEDGMENTS

We thank Dr. H. Kersters-Hilderson (University of Ghent) for the gift of anhydroxylitol and Prof. S. Ogawa (Keio University, Yokohama, Japan) for pseudoglucose. We are indebted to the following persons for their technical assistance in cloning, mutagenesis, protein purification, enzymology, and computer support throughout the project: M. Beyeart, C. Opsomer, J. Seurinck, F. Dardenne, R. Van Cauwenberghe, I. Van den brande, A. M. Van Den Broeck, A. van Vliet, and P. Berthet. We acknowledge help from the scientific and technical staff of LURE (Orsay, France) in crystallographic data collection and processing. We also thank S. De Moor for valuable help in preparing the manuscript. All color figures were obtained using the BRUGEL package.

REFERENCES

Alber, T., Banner, D. W., Bloomer, A. C., Petsko, G. A., Phillips, D. C., Rivers, P. S. & Wilson I. A. (1981) *Philos. Trans. R. Soc. London, B 293*, 159–171.

Bernstein, F. C., Koetzle, T. F., Williams, G. J. B., Meyer, E. F., Jr., Brice, M. D., Rodgers, J. R., Kennard, O., Shimanouchi, T., & Tasumi, M. (1977) *J. Mol. Biol. 112*, 535–543.

Callens, M., Tomme, P., Kersters-Hilderson, H., Cornelis, R., Vangrysperre, W., & De Bruyne, K. (1988) *Biochem. J. 250*, 285–290.

Carrell, H. L., Rubin, B. H., Hurley, T. J., & Glusker, J. P. (1984) *J. Biol. Chem. 259*, 3230–3236.

Carrell, C. J., Carrell, H. L., Erlebacher, J., & Glusker, J. P. (1988) *J. Am. Chem. Soc. 110*, 8651–8656.

Carrell, H. L., Glusker, J. P., Burger, V., Manfre, F., Tritsch, D., & Biellmann, J. F. (1989) *Proc. Natl. Acad. Sci. U.S.A. 86*, 4440–4444.

Chothia, C., & Lesk, A. M. (1986) *EMBO J. 5*, 823–826.

Collyer, C. A., & Blow, D. M. (1989) *Proc. Natl. Acad. Sci. U.S.A. 87*, 1362–1366.

Collyer, C. A., Henrick, K., & Blow D. M. (1990) *J. Mol. Biol. 212*, 211–235.

Dauter, Z., Dauter, M., Hemker, J., Witzel, H., & Wilson, K. (1989) *FEBS Lett. 247*, 1–8.

Dumortier, L., Van der Eycken, J., & Vandewalle, M. (1989) *Tetrahedron Lett. 30*, 3201.

Farber, G. K., Petsko, G. A., & Ringe, D. (1987) *Protein Eng. 1*, 459–466.

Farber, G. K., Glasfeld, A., Tiraby, G., Ringe, D., & Petsko, G. A. (1989) *Biochemistry 28*, 7289–7297.

Hendrickson, W. A. (1985) in *Methods in Enzymology—Diffraction Methods for Biological Molecules, Part B* (Wyckoff, H. W., Hirs, C. H. W., & Timasheff, S. N., Eds.) pp 252–270, Academic Press Inc., London.

Hendrikson, W. A., & Konnert, J. H. (1980) in *Computing in Crystallography* (Diamond, R., Ramesseshan, S., & Venkatesan, K., Eds.) pp 1301–1323, Indian Academy of Sciences, Bangalore.

Henrick, K., Blow, D. M., Carrell, H. L., & Glusker, J. P. (1987) *Protein Eng. 1*, 467–469.

Henrick, K., Collyer, C. A., & Blow, D. M. (1989) *J. Mol. Biol. 208*, 129–157.

Jones, T. A. (1985) in *Methods in Enzymology—Diffraction Methods for Biological Molecules, Part B* (Wyckoff, H. W., Hirs, C. H. W., & Timasheff, S. N., Eds) pp 157–171, Academic Press Inc., London.

Kersters-Hilderson, H., Callens, M., Van Opstal, O., Vangrysperre, W., & De Bruyne, K. (1987) *Enzyme Microb. Technol. 9*, 145–148.

Kim, H. S., & Jeffrey, G. A. (1969) *Acta Crystallogr. B25*, 2607–2613.

Lambeir, A.-M., Lauwereys, M., Stanssens, P., Mrabet, N. T., Snauwaert, J., van Tilbeurgh, H., Matthyssens, G., Lasters, I., De Maeyer, M., Wodak, S. J., Jenkins, J., Chiadmi, M., & Janin, J. (1992) *Biochemistry* (second of three papers in this issue).

Leslie, A. G. W. (1987) *Acta Crystallogr. A43*, 134–136.

Luzzati, V. (1952) *Acta Crystallogr. 5*, 802–810.

Mrabet, N. T., Van den Broeck, A., Van den brande, I., Stanssens, P., Laroche, Y., Lambeir, A.-M., Matthyssens, G., Jenkins, J., Chiadmi, M., van Tilbeurgh, H., Rey, F., Janin, J., Quax, W. J., Lasters, I., De Maeyer, M., & Wodak, S. J. (1992) *Biochemistry 31*, 2239–2253.

Ogawa, S., Tsukiboshi, Y., Iwasawa, Y., & Suami, T. (1985) *Carbohydr. Res. 132*, 77–89.

Rey, F., Jenkins, J., Janin, J., Lasters, I., Alard, P., Claessens, M., Matthyssens, G., & Wodak, S. (1988) *Proteins 4*, 165–172.

Rose, I. A. (1981) *Philos. Trans. R. Soc. London, B 293*, 131–143.

Saman, E., Claeyssens, M., & De Bruyne, C. K. (1972) *Carbohydr. Res. 24*, 173–174.

Stanssens, P., Opsomer, C., McKeown, Y. M., Kramer, W., Zabeau, M., & Fritz, H. J. (1989) *Nucleic Acids Res. 17*, 4441–4454.

Stuart, D., & Walker, N. (1979) *Acta Crystallogr. A35*, 925–933.

Sudfeldt, C., Schäffer, A., Kägi, J. H. R., Bogumil, R., Schultz, H. P., Wulff, S., & Witzel, H. (1990) *Eur. J. Biochem. 193*, 863–871.

van Tilbeurgh, H., Jenkins, J., Chiadmi, M., Janin, J., Wodak, S. J., Mrabet, N. T., & Lambeir, A.-M. (1992) *Biochemistry* (third of three papers in this issue).

Whitlow, M., Howard, A. J., Finzel, B. C., Poulos, T. L., Winborne, E., & Gilliland, G. L. (1991) *Proteins: Struct., Funct., Genet. 9*, 153–173.